Rapid fabrication of interdigitated electrodes by laser ablation with application to electrokinetically enhanced surface plasmon resonance imaging

Larry O'Connell, Brice Poirier, Oleksii Bratash, Charlène Plénière, Loïc Leroy, Yoann Roupioz, Pierre Marcoux

▶ **To cite this version:**

Larry O'Connell, Brice Poirier, Oleksii Bratash, Charlène Plénière, Loïc Leroy, et al.. Rapid fabrication of interdigitated electrodes by laser ablation with application to electrokinetically enhanced surface plasmon resonance imaging. Optics and Laser Technology, 2023, 161, pp.109167. 10.1016/j.optlastec.2023.109167 . hal-03945149

HAL Id: hal-03945149
https://hal.science/hal-03945149

Submitted on 18 Jan 2023

HAL is a multi-disciplinary open access archive for the deposit and dissemination of scientific research documents, whether they are published or not. The documents may come from teaching and research institutions in France or abroad, or from public or private research centers.

L'archive ouverte pluridisciplinaire **HAL**, est destinée au dépôt et à la diffusion de documents scientifiques de niveau recherche, publiés ou non, émanant des établissements d'enseignement et de recherche français ou étrangers, des laboratoires publics ou privés.

Optics and Laser Technology

Rapid Fabrication of Interdigitated Electrodes by Laser Ablation with Application to Electrokinetically Enhanced Surface Plasmon Resonance Imaging

--Manuscript Draft--

Manuscript Number:	
Article Type:	Research Paper
Section/Category:	Laser Materials Processing
Keywords:	Laser Ablation; Rapid Prototyping; dielectrophoresis; electro-osmosis; Surface plasmon resonance; biosensing
Corresponding Author:	Pierre R. Marcoux French Alternative Energies and Atomic Energy Commission FRANCE
First Author:	Larry O'Connell
Order of Authors:	Larry O'Connell
	Brice Poirier
	Oleksii Bratash
	Charlène Plénière
	Loïc Leroy
	Yoann Roupioz
	Pierre R. Marcoux
Abstract:	Significance Dielectrophoresis, electro-osmosis, and other electrokinetic effects are frequently used in a variety of applications but necessitate patterning of electrodes on sensor surfaces. This typically requires a cleanroom and time-consuming, expensive, and arcane lithography and etching procedures. Aim To demonstrate the applicability of commercial laser direct writing equipment for rapid patterning of electrodes into gold layers on glass substrates, particularly with application to producing electrokinetically active plasmonic sensors. Approach A commercial printed circuit board prototyper was used to pattern interdigitated electrode (IDE) arrays into the surface of gold-coated slides and off-the-shelf surface plasmon resonance (SPR) prisms. The electrode geometries resulting from different patterning parameters were characterized by profilometry and electron microscopy. The patterned surfaces were then employed for trapping and electro-kinetic manipulation of bacteria, and finally for sensing of bacteria by SPR imaging. Results Fabrication of an IDE array can be completed in as little as 12 seconds, with longer fabrication times permitting superior geometry and minimum feature size of 15 μm. The patterned IDEs were capable of concentrating bacteria and controlling their position on the sensor surface as a function of applied frequencies. SPR was demonstrated to detect specific interactions between bacteria and immobilized antimicrobial peptides. Conclusions Laser direct writing is demonstrated as a feasible, cleanroom-free alternative to more lengthy lithography methods, permitting very rapid fabrication and prototyping of IDEs, which are compatible with active plasmonic sensing and bacterial detection.
Suggested Reviewers:	Seung-Woo Kim Korea Advanced Institute of Science and Technology swk@kaist.ac.kr Prof. Seung-Woo Kim is an authorof a paper concerning ablation of metal thin films. Furthermore, his work centers on biophotonics, and so the biosensing aspect of our article will also be relevant to his expertise.
	Stavros Chatzandroulis NCSR Demokritos stavros@imel.demokritos.gr Dr. Chatzandroulis is an author on a paper concerning fabrication of interdigitated electrodes for capacitive microsystems in biological sensing

Powered by Editorial Manager® and ProduXion Manager® from Aries Systems Corporation

	Dong Wu Hefei University of Technology dongwu@ustc.edu.cn Dong Wu is an author of a well-cited review of femtosecond laser direct writing.

Powered by Editorial Manager® and ProduXion Manager® from Aries Systems Corporation

Highlights

- Commercial laser direct writing equipment was investigated for rapid patterning of electrodes into gold layers on glass substrates.
- The patterned surfaces were then employed for trapping and electro-kinetic manipulation of bacteria, and finally for sensing of bacteria by SPR imaging
- It constitutes a feasible, cleanroom-free alternative to more lengthy lithography methods.

Manuscript File Click here to view linked References

Rapid Fabrication of Interdigitated Electrodes by Laser Ablation with Application to Electrokinetically Enhanced Surface Plasmon Resonance Imaging

Larry O'Connell[1,2], Brice Poirier [3], Oleksii Bratash [2], Charlène Plénière[2], Loïc Leroy [2], Yoann Roupioz[2], Pierre R. Marcoux[1,*]

[1] Univ. Grenoble Alpes, CEA, LETI, F38054 Grenoble, France

[2] Univ. Grenoble Alpes, CNRS, CEA, IRIG, SyMMES, 38000 Grenoble, France

[3] Y.Spot, CEA, F38054 Grenoble, France

[*]Correspondence: pierre.marcoux@cea.fr; Tel.:+33-4-38-78-15-04

Keywords: Fabrication, laser ablation, rapid prototyping, dielectrophoresis, electro-osmosis, antimicrobial peptides, surface plasmon resonance, biosensing

Abstract

Significance: Dielectrophoresis, electro-osmosis, and other electrokinetic effects are frequently used in a variety of applications but necessitate patterning of electrodes on sensor surfaces. This typically requires a cleanroom and time-consuming, expensive, and arcane lithography and etching procedures.

Aim: To demonstrate the applicability of commercial laser direct writing equipment for rapid patterning of electrodes into gold layers on glass substrates, particularly with application to producing electrokinetically active plasmonic sensors.

Approach: A commercial printed circuit board prototyper was used to pattern interdigitated electrode (IDE) arrays into the surface of gold-coated slides and off-the-shelf surface plasmon resonance (SPR) prisms. The electrode geometries resulting from different patterning parameters were characterized by profilometry and electron microscopy. The patterned surfaces were then employed for trapping and electro-kinetic manipulation of bacteria, and finally for sensing of bacteria by SPR imaging.

Results: Fabrication of an IDE array can be completed in as little as 12 seconds, with longer fabrication times permitting superior geometry and minimum feature size of 15 µm. The patterned IDEs were capable of concentrating bacteria and controlling their position on the sensor surface as a function of applied frequencies. SPR was demonstrated to detect specific interactions between bacteria and immobilized antimicrobial peptides.

Conclusions: Laser direct writing is demonstrated as a feasible, cleanroom-free alternative to more lengthy lithography methods, permitting very rapid fabrication and prototyping of IDEs, which are compatible with active plasmonic sensing and bacterial detection.

Introduction

Interdigitated electrodes – intermeshed, individually addressable planar electrodes – have been demonstrated in a wide variety of applications including biosensing[1,2], cell-sorting[3], diagnostics[4], and petrochemistry[5]; making use of transduction mechanisms either inherent to the electrodes themselves (*e.g.*, impedance[4,5] or capacitance based methods[6–8]) or in adjacent transducers near which the IDEs concentrate an analyte by electrokinetic mass transport.[9,10]

When employed for mass transport, IDEs can leverage electrokinetic effects such as dielectrophoresis (DEP), alternating current electro-osmosis (ACEO), and the electro-thermal effect (ETE) to concentrate and displace particulate matter in a carrier liquid as a function of the frequency and amplitude of oscillating electrical signals applied to the opposing electrodes.[9,10]

Due to the polyvalent nature of IDEs, they are incorporated into a large variety of different devices. As a result, it is common practise for researchers to fabricate the IDEs themselves in order to tailor the micro-patterned surfaces to their specific application.[5,7–9,11]

Traditionally, fabrication of electrodes necessitates some or all of: deposition of the electrode material and adhesion layers onto a suitable substrate, fabrication of a hard mask, and deposition of photoresist followed by lithography and associated wet or dry etching techniques.[12–15] Such methods are time-consuming, expensive, and incompatible with rapid iteration of component design, slowing the pace of research and obligating researchers to handle etchant chemicals and perform lengthy lithography processes and other steps which require skills that may be unrelated to their scientific training.

Increasingly, there is interest in more rapid processes for producing patterned surfaces. Alternative methods that have been demonstrated include inkjet printing,[16] fused deposition modelling,[17] and laser ablation of printed circuit boards (PCBs).[18] Although intriguing results have been obtained with these methods, each suffers from various drawbacks including poor pattern reproduction, large minimum feature sizes, large variability that depend on fabrication parameters etc.

Furthermore, use of unorthodox materials to form the IDEs may prove incompatible with popular bioconjugation methods such as thiol-gold immobilization[19,20], introducing complication downstream of the IDE fabrication.

First proposed by Tender *et al.* [21], laser direct writing (LDW) has only rarely been exploited for the fabrication of IDEs, despite the advantage that LDW can surpass the achievable resolution offered by conventional photolithography of gold.[22] However, fabrication of IDEs by laser ablation has so far necessitated construction of a custom optical setup, typically by channelling laser output *via* a dedicated optical bench through adapted microscope objectives.[21,22] While elegant, this method substitutes lengthy fabrication protocols with the necessity to develop a custom optical system, negating any time-saving and recreating the problem of obligating experimenters to develop skills orthogonal to their research.

In order to improve the turn-around time for rapid prototyping of IDEs, here is presented a patterning method based on laser ablation of a deposited metal layer on glass substrates by a commercial PCB prototyper. This method retains the time-saving benefits of LDW, without the need to develop a custom optical setup.

In order to demonstrate the compatibility of the fabricated IDEs with biosensing, they were first employed for mass concentration of bacteria in a microfluidic circuit, then the same geometry was

patterned into a surface plasmon resonance imaging (SPRi) sensor functionalized with antimicrobial peptides (AMPs) (Figure 1).

SPR is a popular technique for label-free, real-time monitoring of surface phenomena, transducing mass-uptake at a sensor-analyte interface into an optical signal.[23] SPR imaging builds on the strength of SPR by observing the entire surface of a sensor that has been functionalized with many different ligands, simultaneously monitoring the interaction of each functionalized region in a single, parallel, multiplexed assay.[24,25] SPRi has been demonstrated for the specific detection of bacteria using arrays of immobilized AMPs.[26] However, the time-to-results with this method was long, taking several hours to reveal interactions between AMPs and challenge bacteria.

Recently, there is increasing interest in enhancement by electrokinetic mass transport of plasmonic sensors including SPR[27], localized SPR[28], and optical fiber SPR sensing[29]. The work of Costella *et al.* and Avenas *et al.* demonstrated a form of active plasmon SPRi sensing on IDE arrays but stopped short of chemical functionalization of the surface for specific sensing.[9,10] Terao developed this technique for the monitoring of specific interactions between immunoglobulin G (IgG) and sensor-immobilized anti-IgG antibodies.[14]

To the authors' knowledge, this work represents the first time that LDW has been used to rapidly fabricate electrodes directly into an SPR sensor; and furthermore, the first time electrokinetic SPR imaging (EK-SPRi) has been demonstrated for parallel, multiplexed sensing with multiple probes of a clinically relevant, antibiotic-resistant strain of *Staphylococcus aureus*.

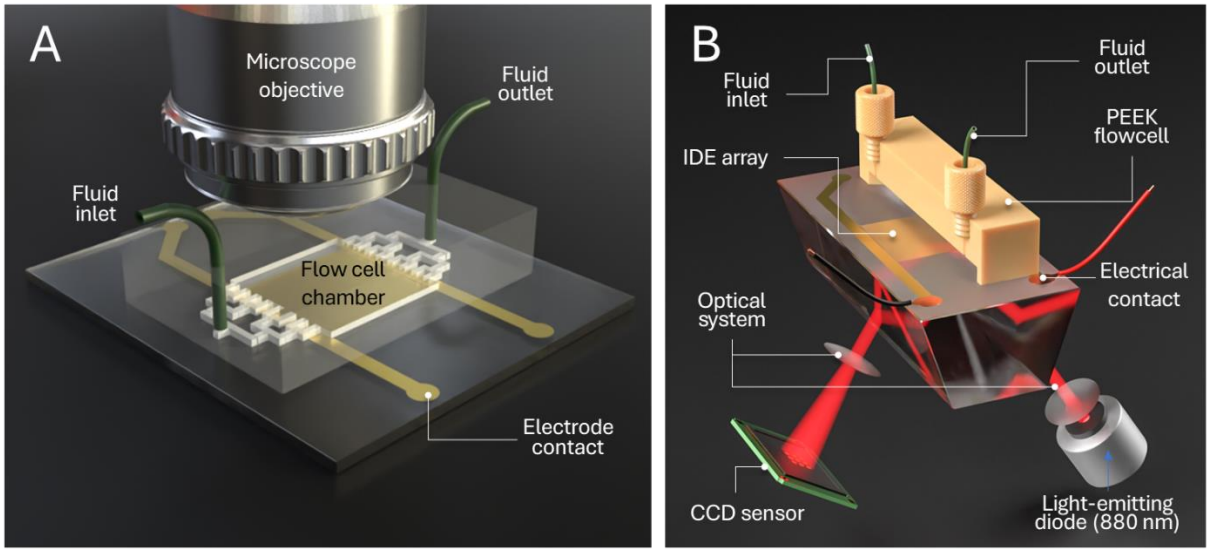

Figure 1 (A) An illustration of the electrotrapping experimental setup. An interdigitated electrode array was patterned into the surface of a gold-coated slide, interfaced with a PDMS flow cell, and observed by microscope. (B) Illustration of the electrokinetic SPR imaging system in the Kretschmann configuration with a cutaway of the flow cell.

Materials & Methods

Purchased materials

Dimethylformamide (DMF), dimethyl Sulfoxide (DMSO), ethanol (≥99.9%), glycerol (≥99%), phosphate-buffered saline (PBS), polydimethylsiloxane (PDMS; Sylgard 184), poly(ethylene glycol) methyl ether thiol (PEG-800), potassium nitrate (KNO_3), and trypticase soy broth (TSB) were purchased from Sigma-Aldrich (Saint Quentin Fallavier, France) and used without additional purification. 0.9% w/v NaCl solution (OTEC) was purchased from VWR (France). Deionized water (DIW; >18 MΩ resistivity) was obtained from an ELGA PURELAB flex dispenser (Veolia Water, France).

Peptide synthesis

Magainin was synthesized by Smart Bioscience (Saint Égrève, France) using a standard Fmoc solid-phase method described elsewhere.[26] The remaining peptides were synthesized by the 9-fluorenylmethoxycarbonyl/tert-butyl (Fmoc/tBu) strategy on RINK-amide resins on a Syro II peptide synthesizer (Biotage), followed by purification by reverse phase HPLC. Purity of synthesized proteins was confirmed by high-performance liquid chromatography and electrospray ionisation mass spectrometry. While magainin is conjugated *via* an L-cysteine amide on the C-terminus, the remaining peptides are instead conjugated *via* 3-mercaptoproprionic acid (3-MPA) on their N-terminus. Further information on antimicrobial peptides can be found in **Supplementary Table 1**.

Bacterial culture

Bacterial strain *Pseudomonas putida* (ATCC 12633) was obtained from the *Félix d'Hérelle Reference Center for Bacterial Viruses* of Université Laval, Quebec, Canada. Bacterial strain *S. aureus* subsp. *aureus* Rosenbach (ATCC 43300) was obtained from Microbiologics (Kwik-Stik™ lyophilized strains). Bacterial cultures were routinely prepared in TSB at recommended temperatures for each host: *S. aureus* at 37 °C and *P. putida* at 30 °C.

Preparation of gold substrates

Flat *D*263® glass slides coated with Cr/Au – 1.5 ± 0.5 nm / 55 ± 3 nm were purchased from SCHOTT and cleaved into 30×26 mm sections. Gold-covered SPRi biochips were purchased from Horiba Scientific (Palaiseau, France).

Rapid fabrication by laser ablation

Gold slides and prisms were both patterned in the same manner using a ProtoLaser S4 printed circuit board prototyper (LPKF, Garbsen Germany), which was initialized at least 20 minutes before use to allow the laser to reach stability.

Laser power was set to 5 W for hatching and 9 W for contouring. Both hatching and contouring were performed with a pulse frequency of 160 kHz. Insulation width was maintained at 15 µm. Several laser patterning parameters were varied in order to find the optimal conditions for reproduction of the smallest possible features of a pattern design. Parameters varied included the hatching overlap (10, 15, 20, or 25 µm), repetition of beam passes (1, 2, or 3 passes), and the direction of the beam (concentric, parallel, or perpendicular to the electrode axis).

The pattern design features 54 electrodes fingers, 27 connected to each of two separate opposing busbars (**Supplemental Figure S1**). The busbar width was 1 mm to minimize voltage drop across this part of the circuit. The electrodes overlapped by 7.7 mm of their total 8 mm length. As well as

varying fabrication parameters, the pattern design was also varied to include different electrode widths (30, 50, or 100 µm) and electrode separations (15, 20, 30, 40, and 50 µm).

After optimization of the patterning parameters, the best settings were used to produce electrokinetic SPRi prisms (EK-SPRi prisms)

Electron microscopy

In order to evaluate the fidelity to pattern designs and efficacy of removal of gold from ablated regions, scanning electron microscopy (SEM) was carried out on substrates produced by different patterning parameters. The surfaces were observed using a Zeiss Ultra 55 scanning electron microscope under a 2 kV acceleration voltage and working distance in the range 5-10 mm. Images were obtained with either an "in-chamber" secondary electron (SE) detector or an "in-lens" detector mounted inside the column, yielding greater topographical contrast.

Profilometry

Profilometry measurements were performed on patterned surfaces using a DektakXT profilometer equipped with a 12.5 µm-radius stylus applying a 3 mg stylus force. Measurements were taken both perpendicular and parallel to the electrode axes.

Simulation

Clausius–Mossotti (CM) factors were calculated using the software tool myDEP[30] for a range of carrier liquid conductivities and electrical field oscillation frequencies, using a two-shell cell model.[10]

Electrokinetic trapping and concentration

A microfluidic flow cell was produced by pouring vacuum-degassed PDMS over a stainless-steel mould, followed by curing at 80 °C for 90 minutes. The fabricated flow cell consisted of an inlet and outlet, each subdivided into 16 channels using 4 layers of T-junctions on either side of a main chamber 200 µm in height (Figure 1A). This geometry allows an homogenous flow of analyte through the chamber and thus over the IDE array.

The high reflectivity of the gold electrodes necessitated observation from above (*i.e.*, from the side of the PDMS circuit). However, the thickness of the PDMS necessitated a larger working distance than would be possible with a microscope objective that would permit the magnification needed to observe trapping of individual cells. To circumvent this, the patterned slide was interfaced with the PDMS flow cell and mounted in a microscope permitting single-cell resolution (× 500-600 magnification) over the width of one electrode finger while permitting a working distance longer than the thickness of the PDMS layer (Figure 1A).

Using a syringe pump (KDS 250 Nanoliter 4, KD Scientific), a flow rate of 0.4 mL/min was used to fill the PDMS circuit with bacterial suspensions, and a reduced flow rate of 0.1 mL/min during electrokinetic experiments. The salt concentration of the carrier liquid was varied between 1.54 mmol and 154 mmol NaCl (*i.e.*, physiological saline). Signals were applied between the IDE array contacts, controlled by a signal generator, and monitored using an oscilloscope (waveRunner 64Xi, Teledyne LeCroy). The resulting behaviour of bacterial cells during application of signals was observed and recorded by the microscope camera (Sony α7S).

Imagery was transcoded from Apple ProRes 422HQ using Davinci Resolve v17.4.3, with each frame extracted as a RGB colour TIFF. Frames were then processed by ImageJ (v1.53f51) to perform background subtraction and contrast adjustments.

Immobilization of peptides on electrokinetic prisms

The patterned gold surfaces of EK-SPRi prisms were rinsed with DIW, ethanol, then once more with DIW. EK-SPRi prisms were then dried with argon and plasma cleaned for 3 mins in 0.6 mBar 75:25 oxygen/argon mix at 80% power in a Femto plasma system (Diener electronic, Ebhausen, Germany) and the surface left to stabilize for 24 hours at room temperature.

The surface of each EK-SPRi prism surface was then functionalized with peptides using a protocol described elsewhere.[26] Lyophilized peptides were resuspended (Magainin in DMSO, others in PBS supplemented with 5% w/v glycerol) at 1-2 mmol and stored at −80 °C. 20 µL aliquots of peptides were sonicated for 10 minutes in an ultrasound bath to disaggregate them, then centrifuged for 2 000 *g* for 20 seconds at room temperature. Peptides were then diluted to 100 µmol by addition of aqueous solution of 15% w/v DMF, 15% w/v glycerol to make a final volume of 20 µL. Peptide suspensions were then once more centrifuged as before, sonicated a further 5 minutes as before, then centrifuged again before deposition on the prism surface.

The surface texture created by laser patterning caused deposited droplets to spread across the surface by capillary action. To permit localized functionalization, the EK-SPRi prisms surface was partitioned into sections by application of silicon grease using the edge of a microscope cover glass, creating a hydrophobic barrier on the surface to yield eight separated regions available for functionalization. 1 µL of each peptide suspension was pipetted onto a different region and the suspensions incubated with the prism surface for 18 hours at 25 °C in the dark in a humid environment inside a desiccator loaded with saturated KNO_3 solution (to produce 95% relative humidity).

The following day, the prism surface was rinsed with DMF then DIW. The prism was then dried with argon and immediately covered with 2 mmol PEG-800 aqueous solution and incubated for 2 hours at 25 °C in the dark in a humid chamber, blocking the surface. The prism was then rinsed with once more with DIW, dried with argon, and stored in air in a 50 mL Falcon tube in the dark at 4 °C for 24 hours before use.

Peptide-bacteria interaction monitoring by surface plasmon resonance imaging

The detection of immobilized AMP interaction with bacteria was performed using a commercial SPRi device (Horiba Scientific, Orsay, France) placed in an incubator at 30 °C. The SPRi chip was interfaced with a PEEK flow cell to allow interaction with the bacterial suspension (Figure 1B). The biochip surface was illuminated from below with polarized and collimated 880 nm light from a light-emitting diode. Monitoring of binding was performed using a CCD camera (Dolphin F-145B, Allied Vision, Stadtroda, Germany) with a fixed working angle of 52.78°.

An exponential-phase culture of *S. aureus* was pelleted by centrifugation at 5 500g at room temperature for 5 minutes, resuspended in 1.54 mmol NaCl solution to a concentration of 10^9 CFU/mL, centrifuged and resuspended a second time in 1.54 mmol NaCl, then adjusted to various concentrations between 10^6 – 10^8 CFU/mL and introduced to the sensor surface with a flow rate of 4 µL/s. Images were taken every six seconds.

In order to facilitate mass transfer to the surface, the frequencies established in earlier electro-trapping experiments were applied to the EK prism contacts. First, a signal of 100 kHz 5 V_{pp} is applied for 10 s to facilitate mass transport of bacteria from the analyte suspension (pDEP interval). Then, a signal of 10 kHz 5 V_{pp} is applied for a further 10 s in order to move any captured bacteria to the center of electrode fingers (ACEO interval). Finally, no signal was applied for 40 seconds to allow bacteria to interact with immobilized AMPs (interaction interval). These signals were applied in

sequence of five cycles after each injection of bacteria and the SPR signal allowed to stabilize for 10 minutes to reveal any mass uptake on the electrode surfaces.

Data analysis

SPRi reflectance images were recorded with an SPRiLab SPR imager (Horiba Scientific, Palaiseau, France). Data were treated using SPRiView (v3.1.2) and processed using MatLab R2021a (v9.10). Regions of interest (ROIs) were manually identified during initialization of the SPRi experiment, chosen to correspond to the phage-functionalized regions of electrode centers of the surface.

Since the ROIs exhibited plasmon curves with different slopes at the chosen working angle (**Supplementary Figure S3**), it was not appropriate to directly compare the changes in reflectivity between different ROIs but rather the shift in the plasmon curve corresponding to the reflectivity change. In order to calculate the plasmon curve shift, a B-spline was fitted to the plasmon curves observed at the beginning of the SPR experiment. This fit was then used to convert changes in reflectance to the real plasmon curve shift, expressed in degrees.

A one-minute rolling average of plasmon angle shift (*i.e.*, a mean of 10 data points) was plotted for analysis of interactions between AMP and bacteria. All curves were offset to zero approximately one minute prior to injection of bacterial suspensions, and corrected for baseline drift.

Theory

Principle of dielectrophoresis

Dielectrophoresis (DEP) is a phenomenon whereby particles in an electrolyte medium will experience a nett motive force in response to an inhomogeneous electrical field. For a homogenous particle, the time-averaged DEP force on a particle of radius *r* due to an electric field gradient $\nabla|E^2|$ is given by[31]:

$$\langle \vec{F}_{DEP} \rangle = 2\pi r^3 \varepsilon_0 \varepsilon_m Re\{CM(\omega)\} \nabla \left|\vec{E}\right|^2 \qquad (1)$$

Where ε_0 is the permittivity of free space, ε_m is the permittivity of the medium, and $Re\{CM(\omega)\}$ refers to the real component of $CM(\omega)$ — the *Clausius-Mossotti* (CM) *factor* as a function of ω, the angular frequency of oscillation of the electrical field.

Crucially, the force is proportional to the gradient of the square of the electric field but not on its polarity. This permits us to leverage DEP to concentrate bacteria from the bulk onto the electrode borders by applying an alternating current with a frequency that yields a positive CM factor.

For a given electrical field oscillation frequency, the sign of the CM factor depends strongly on the medium conductivity, the particle's geometry, and its electrical permittivity. Figure 2 shows the balance of forces on a homogenous, spherical particle in an electric field gradient. When the particle is more polarizable than the surrounding medium, the resulting force is towards the region of high field gradient, a regime known as positive dielectrophoresis (pDEP). Conversely, a less polarizable particle than the surrounding medium experiences negative dielectrophoresis (nDEP) — a force away from the region of high field gradient.

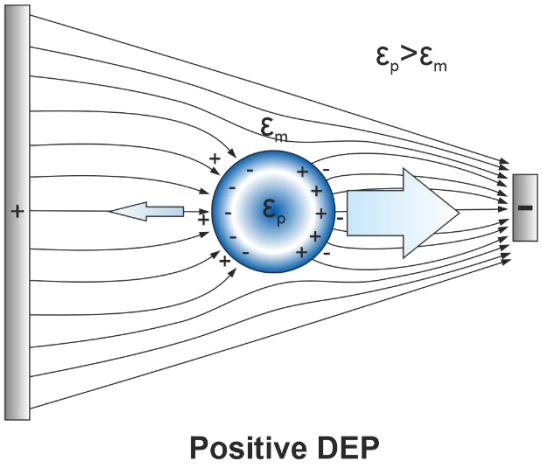

Figure 2 Schematic representation of positive dielectrophoresis for an homogenous, spherical particle in an electric field gradient. A particle that is more polarizable than the medium experiences a force towards the region of high electric field gradient.

While Figure 2 depicts the case for a spherical and homogenous particle, the CM factor for a bacterium is more complicated since the cell is composed of a series of cell membranes enclosing a cell cytosol. Two bacterial strains were used in this work — *P. putida* and *S. aureus*. Although *S. aureus* is Gram-positive and so differs in cell wall composition compared to Gram-negative, *P.*

putida; in practice the convention is to neglect the intermediate layer of Gram-negative bacteria from calculations of the CM factor since it is only 2 nm thick. This permits the use of a more simple, two-shell model for both bacteria, specifying a separate conductivity (σ) permittivity (ε) for each region of the cell.

In order to predict the correct signals to apply to the IDE array in order to manipulate bacterial cells, the software tool myDEP[30] was used to calculate the CM factor for *S. aureus* and *P. putida* over a range of carrier liquid conductivities and electrical field oscillation frequencies from 1 kHz to 1 GHz (Figure 3). A positive CM factor — and thus pDEP — was obtained in the frequency range 1 kHz to 100 MHz when the carrier had a conductivity lower than 0.2 S/m, which corresponds to an NaCl concentration of 17.1 mM or lower.

This provides a basis to estimate the experimental conditions necessary to facilitate pDEP and hence concentration of bacteria on the electrodes.

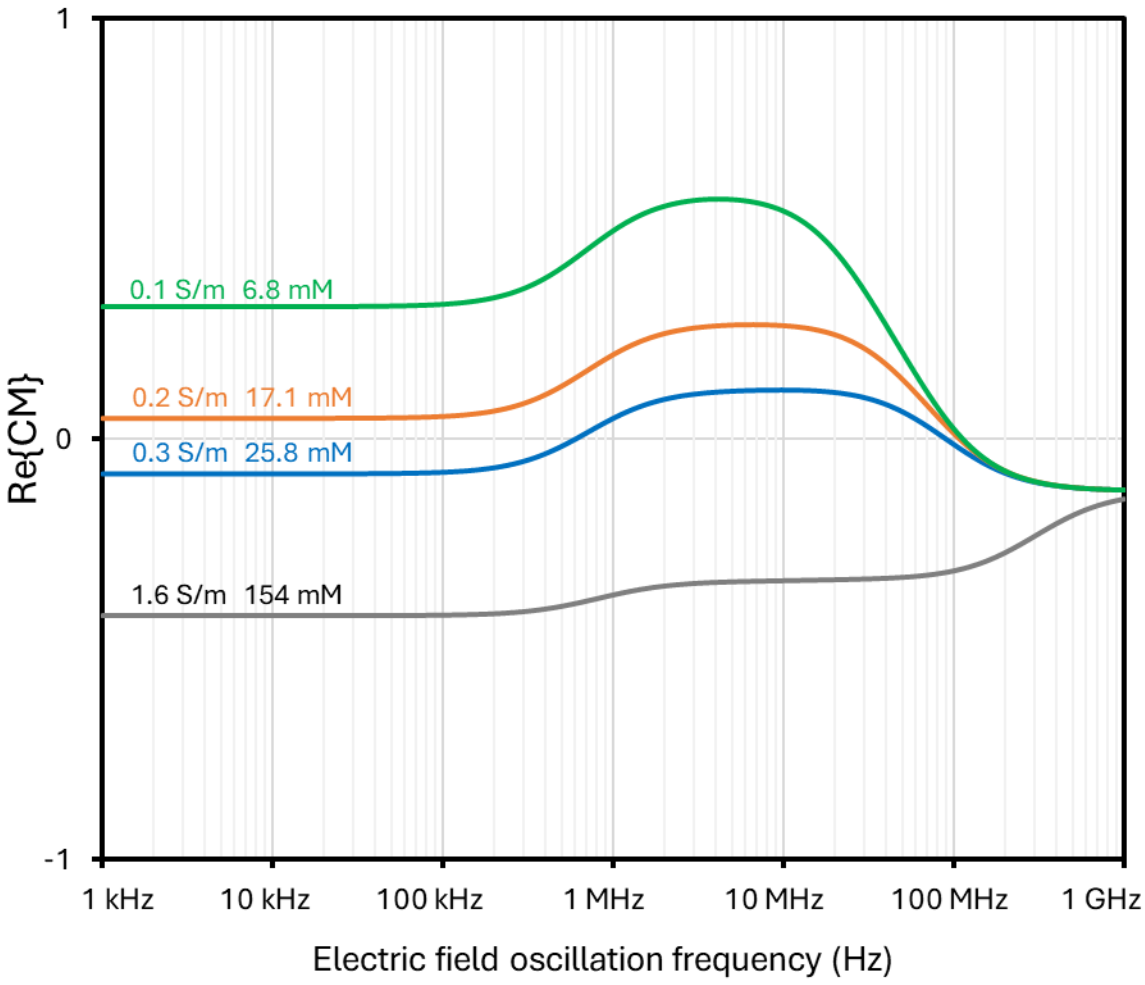

Figure 3 The Clausius-Mosotti (CM) factor, as calculated at a range of frequencies for various medium conductivities assuming a two-shell bacterium model and assuming a negligible volume fraction of the carrier liquid is occupied by suspended cells. An NaCl concentration of 17.1 mM (orange line) yields a positive CM factor over the entire frequency range from 1 kHz to 100 MHz, and thus permits a positive dielectrophoretic force on bacteria.

Principle of alternating current electro-osmosis

In contrast to DEP — which acts on the cells directly — ACEO acts on the carrier liquid itself, creating a current of ions perpendicular to the long axis of the electrode fingers which entrains the carrier fluid — and in turn any suspended particles — *via* drag forces.[32]

A solid surface immersed in an electrolyte presents a given surface potential V_0 and thus spontaneously develops an electric double layer. When a rapidly changing potential is applied between two adjacent electrodes, the surface does not discharge everywhere simultaneously, leading to a tangential component of the electric field $\vec{E}_{||}$. Non-hydrated, charged ions of the medium in the double layer are accelerated by this electric field, away from electrode borders and towards the electrode center.[32]

Ramos *et al.* gave an expression for the fluid velocity $\vec{v}$ across the electrode surface as a function of $\vec{E}_{||}$, the charge density of the double layer σ_q, and the viscosity η:[33]

$$\vec{v} = \frac{\vec{E}_{||}\sigma_q}{\kappa\eta}$$

The fluid velocity thus depends on both the conductivity and the frequency of electric field oscillation. In order to leverage the ACEO effect, a non-zero minimum conductivity is required and the signals applied to the electrodes must be within the frequency interval permitting ACEO.

Results

Electrode patterning

In order to optimize IDE fabrication, electrodes were fabricated with various parameters, imaged by SEM, and compared based on several figures of merit including fidelity to the original CAD design, minimal electrode width and separation, and presence of residual metal in ablated regions or redeposition on un-patterned regions.

Initial patterning attempts made use exclusively of the 'contouring' tool with a concentric path, which specifies a beam route that hugs the periphery of unablated regions and uses a moderate power of 9 W compared to the device's maximum of 12 W, which is normally reserved for milling through the entire substrate thickness.

SEM analysis of these initial patterning experiments revealed that the CAD pattern was reproduced on the surface with reasonable fidelity with an electrode width of 110 µm and electrode separation of 37 µm (Figure 4a and b). Furthermore, gold was effectively removed from between the electrodes. Electrical isolation of the IDEs was later confirmed with a multimeter, which showed no short circuit between opposing electrodes. This first result was all the more interesting since patterning with these settings took approximately 12 seconds (Supplemental video S4).

However, artifacts were observed in certain regions of the IDE array where the pattern geometry necessitated a tight turning circle of the beam path (Figure 4a and b). At the electrode extremities, in between the end of each electrode and the opposing busbar, the concentric contouring tool failed to remove the metal and instead produced a repeated oval motif of resolidified material (Figure 4b). The concentric contouring also failed to remove material at "corners" in the beam path (Figure 4a). Also, although the CAD design specified flat electrode tips, the electrode fingers took on a rounded shape and greater width than the CAD design (Figure 4b). We attributed this to an overshoot of the beam as the device attempted to round the corner at the end of each electrode.

While the metal in between the electrodes was observed to be entirely removed, the electrode borders seem to be subject to pure melting rather than ablation[34], with surface tension of the transiently molten metal forming a 2-4 µm-wide ridge during resolidification.

To explore the possibility of improving electrode geometry and push the resolution limits of the device, subsequent experiments explored the use of multiple repetitions and alternative beam paths. Since it has been shown that reduction of electrode width and separation improves sensitivity with some transduction methods (*e.g.*, impedance[4,35] capacitive sensors[36]), we sought to find the limit of minimum feature size producible with laser ablation in order to demonstrate the wide applicability of this method to a variety of sensor types.

Following the contouring tool with a 'hatching' tool resulted in improved electrode geometry. The hatching tool used a lower power of 5 W and specifies a rastering beam path that proceeds line-by-line across the substrate surface, activating the laser only when over a region marked for ablation by the software. Electrodes of width as thin as 15 µm can be achieved in this way (Figure 4d), much smaller than the 50 µm minimum conductor trace width specified by the manufacturer. However, due to the overshoot problem, the electrode bulges to ~20 µm for the last 200 µm of the electrode length.

Rather than a minimum electrode width, the limiting factor with this device was found to be the finite minimum width of the ablated region. The software of this device (tool library version 0.3.11) will not translate hatching overlap of smaller than 15 µm to the substrate, and instead fails to remove material between electrodes with these settings. Setting the hatching instead to 20 µm is necessary to yield the minimum observed electrode separation of 35 µm. This is reasonable since the manufacturer specifies a minimum focused beam diameter of 20 ± 2 µm.

A poor result was produced when repetitions of two or three passes were specified, since slight variation in the substrate/beam alignment between passes resulted in unpredictable removal of material from the electrode fingers (Figure 4c). It was unclear whether this was due to uncontrolled movement of the substrate relative to the stage, or rather poor translational precision of the stage actuators.

Surprisingly, an improvement was observed when using a hatching path that rastered perpendicularly rather than parallel to the electrode axis (Supplementary Figure S1). It was expected that a parallel beam path (*i.e.*, following the electrode axis) would provide superior results, but instead was found to ablate a wider region and lead to more deposition of metal on un-patterned regions. This may be because a parallel beam path results in the ablation being initiated in adjacent regions consecutively within 6.25 µs, which is of the same order of magnitude as the time scale of heat dissipation out of the focal volume of the laser[37], which may result in energy input into metal that is still molten from ablation of an adjacent region. In contrast, if using a perpendicular beam path, immediately adjacent locations between electrodes are not removed consecutively and instead have time to reach thermal equilibrium with the bulk of the substrate before the next beam pass. We posit that redeposition of gold on un-patterned regions was minimized when a

perpendicular (Figure 4f) instead of parallel hatching path was used (Figure 4e) because molten metal had an opportunity to cool before return of the beam.

Regardless of tool settings, the formation of a ridge persisted at the electrode boundary as a result of ablation of adjacent metal (Figure 4e and f), accompanied by a modified surface texture due to transient melting and resolidification (Figure 4f, black arrow).

Finally, optimal settings were found that resulted in efficient removal of gold from the glass, minimized redeposition of ablated material, and produced consistent electrode widths. For subsequent SPR experiments, IDE arrays were produced 85 μm width electrodes with 45 μm spacing (Figure 4g).

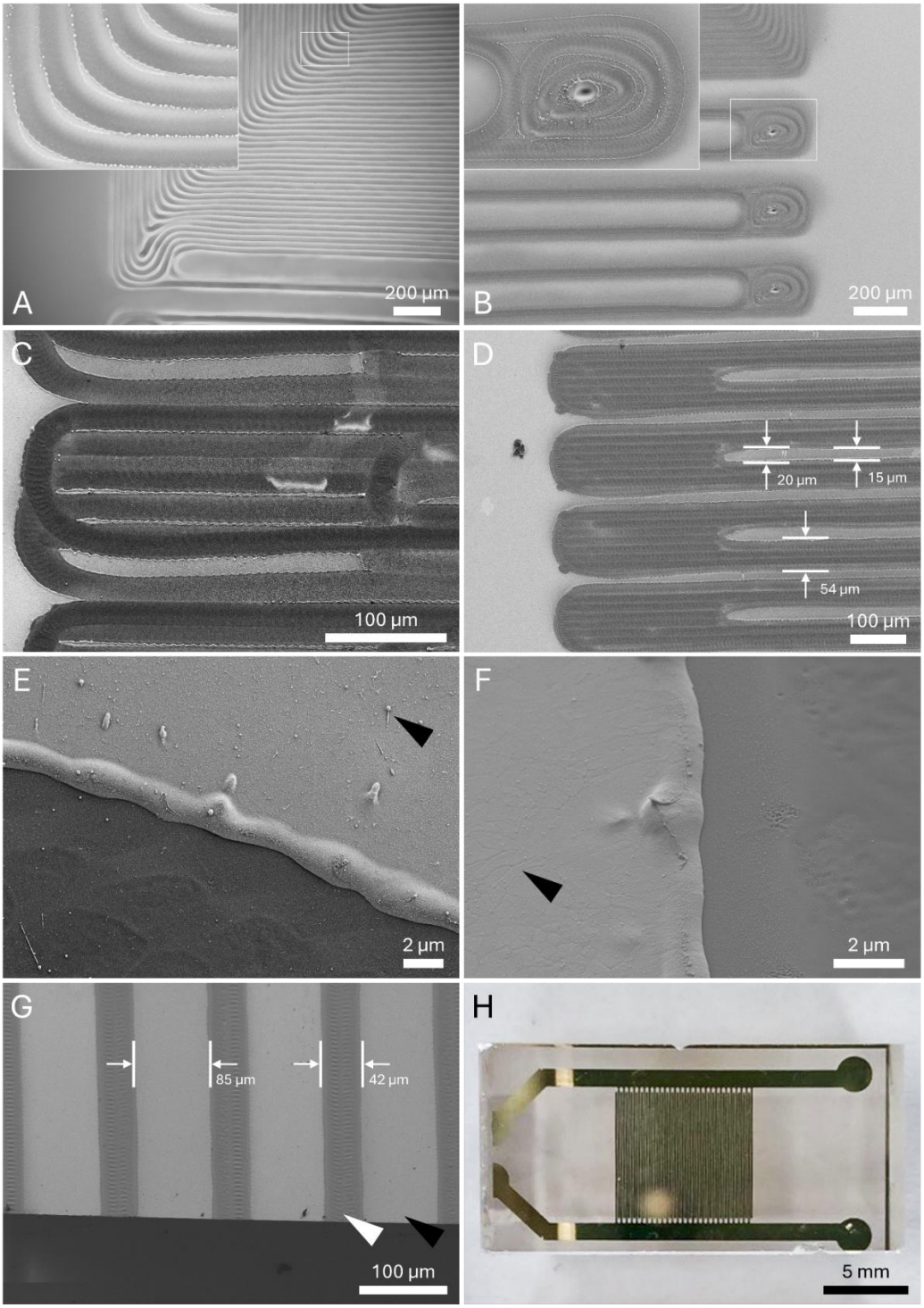

Figure 4 Collage of scanning electron micrographs of IDE arrays resulting from various patterning parameters. (A) Far from the electrode fingers, the concentric contouring path leaves residual metal on the surface where successive passes fail to overlap. Inset shows that this phenomenon is most pronounced in regions where the beam path exhibits high curvature. (B) The concentric contouring path also fails to completely remove metal between the end of each electrode and the opposing busbar. Inset shows detail of the repeating oval motif of resolidified metal. (C) Multiple repetitions of the contouring and hatching paths are poorly superimposed, leading to a failure to transfer the design to the substrate. (D) Combining a contouring pass with a parallel hatching pass can produce electrodes with a width as thin as 15 µm. (E) Electrode boundaries exhibited a raised profile up to 300 nm above the surface and extending up to 4 µm into un-patterned regions. Redeposition of removed metal was observed in surrounding areas (black arrow). (F) Use of a perpendicular hatching path reduced deposition in un-patterned regions but did not mitigate the increased metal thickness at the boundaries. (G) An edge-on cross-sectional view of uniform electrodes of 85 µm width (black arrow) and 42 µm

separation (white arrow), fabricated for use in subsequent surface plasmon resonance experiments. (H) A typical patterned SPRi prism that results from laser ablative patterning.

Profilometry

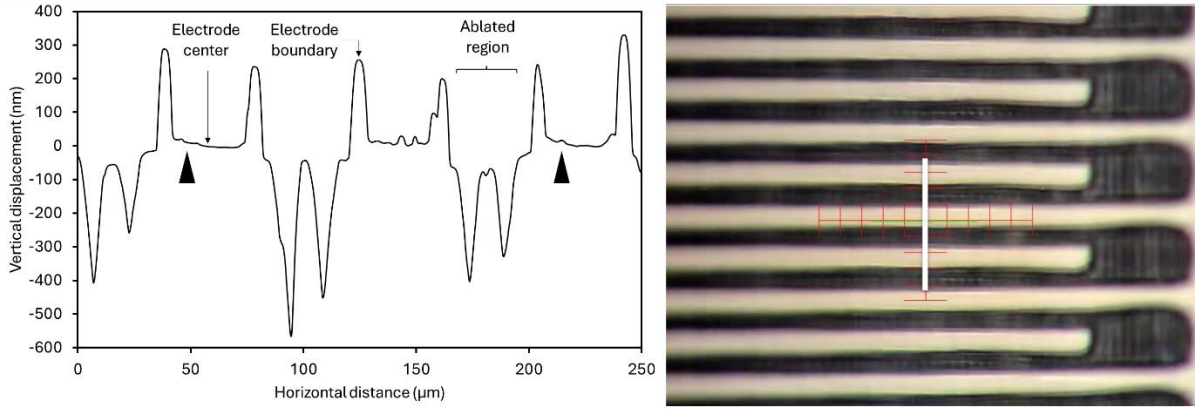

Figure 5 Left: Profilometry analysis of a patterned gold-covered slide, showing the profile perpendicular to the electrodes. Black arrows indicate a small increase in metal layer thickness that extends approximately 15 µm from the boundary towards the electrode center. Note the different scales on the x and y axes, which greatly exaggerates the vertical displacement. Right: Optical microscopy of the region measured. The location of the measured profile is indicated (white line).

In order to obtain a more quantitative picture of the patterned surfaces, profilometry was performed on a patterned slide with 50 µm-wide electrodes. The electrode boundaries were observed to rise approximately 300 nm above the surface, a significant departure from the 56.5 nm nominal thickness of the original metal layer (Figure 5). While profilometry appears to indicate that the boundary ridge of 8 µm width, this is not in agreement with SEM imagery of the same regions (Figure 4e and f). It is likely that the width measured by profilometry was an artifact stemming from a convolution of this surface feature with the 12.5 µm-radius stylus tip, giving an erroneous result for the lateral dimension of the ridge. Instead, we conclude that the vertical displacement of up to 300 nm obtained by profilometry is reliable, while the lateral width of the boundary ridge should instead be measured from electron micrographs (Figure 4e and f), indicating a ~3 µm-thick ridge 300 nm in height.

Also observed was a region that extends ~15 µm into the electrode with a smaller departure from nominal thickness of ~20 nm (Figure 5, black arrows). Favouring electrodes with a width larger than ~50 µm allows rapid fabrication of electrodes with a central region with nominal metal layer thickness unaffected by the ablation process.

In between the electrodes were observed the same repeating circular motif as in SEM, originating from the firing pattern of the laser which removes some glass material below the gold layer to a depth of 200-600 nm. For the purposes of IDE fabrication, the removal of some glass is not deemed to be problematic since this region is not active for surface plasmon resonance nor is it targeted for functionalization.

Electrotrapping

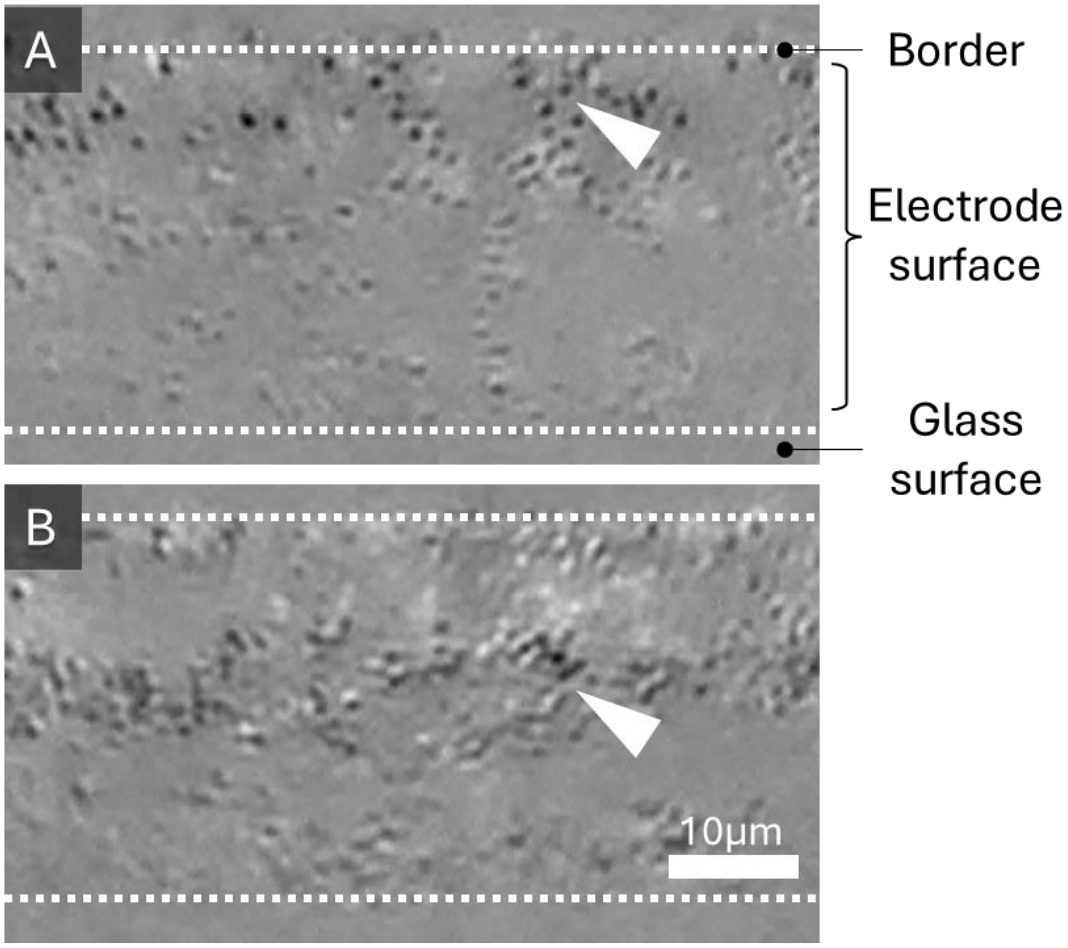

Figure 6 (A) Upon introduction of the *P. putida* and application of alternating electrical signals to the electrode contacts, bacteria (white arrows) were observed to be concentrated at the electrode borders or (C) displaced to the electrode centers, depending on the applied frequency.

In order to confirm the ability of the patterned electrodes to concentrate bacteria from the carrier liquid by pDEP and displace them to the electrode centers using ACEO, a glass slide featuring a patterned IDE array was interfaced with a microfluidic circuit and exposed to *P. putida* at a concentration of 10^8 CFU/mL in carrier liquid of varying ionic strength (0.15 – 15.4 mmol NaCl).

Electrotrapping experiments were performed with *P. putida* as a surrogate for *S. aureus* since the latter is a biosafety level 2 (BSL-2) organism, which prohibits manipulation in lower BSL facilities. Use of *P. putida* simplified manipulation during optimization of applied signals.

Informed by calculations of the CM factor, signals of up to 14 V peak-to-peak (V_{pp}) and frequency between 5 kHz 200 kHz were applied to the electrode contacts and the resulting movement of bacteria observed by optical microscopy.

In this frequency interval, both pDEP and ACEO are expected to occur in superposition, but the balance between them was found to vary depending on the applied frequency. At 100 kHz and above, bacteria were observed to be congregate on the electrode borders within one second (Supplementary video S5). Reducing the signal towards 10 kHz was found to progressively alter the balance of pDEP and ACEO forces, permitting the displacement of bacteria towards the center of the electrode.

The combination of this amplitude and range of frequencies has been shown in similar conditions not to result in electrochemical oxidation of the electrodes.[14]

SPRi

In order to validate the sensing ability of the EK-prisms, an SPRi prism surface was double functionalized, first by patterning to create an IDE and then chemically by covalent immobilization of an array of five AMPs with known affinity to *S. aureus* (the challenge bacteria): bactenecin[38] and a bactenecin derivative[39], cecropin A-melittin[40], penetratin[41], and magainin[42].

A suspension of *S. aureus* was resuspended in 1.54 mmol NaCl solution and introduced to the sensor surface using a microfluidic flow. Following application of signals to the IDE array, a persistent plasmon resonance angle shift was observed on regions functionalized with AMPs, indicating mass uptake on the surface (Figure 7). The degree of shift increased with increasing concentration of bacteria in the range 10^6-10^8 CFU/mL. Application of alternating current to the IDE array results in a transient change in the reflectivity, most likely to Joule heating.

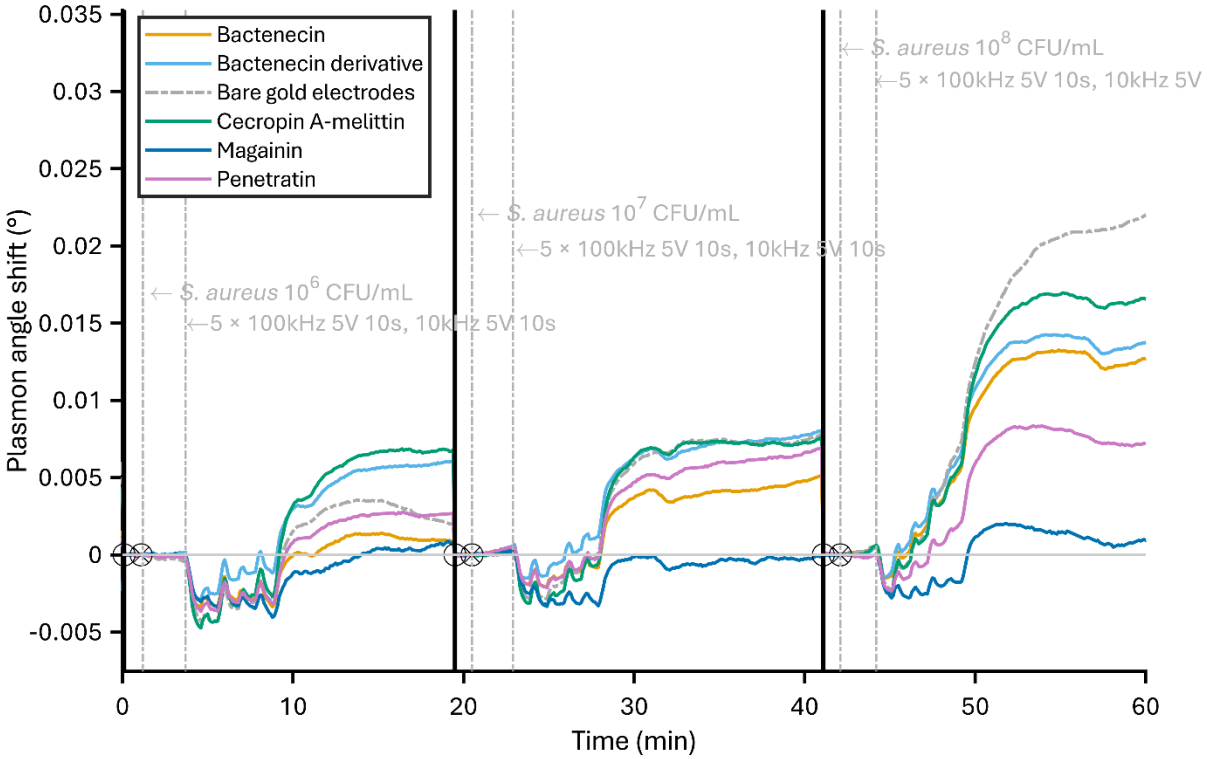

Figure 7 Surface plasmon resonance sensorgrams showing the response of patterned sensor surfaces, functionalized with antimicrobial peptides, to injections of *S. aureus* at 10^6, 10^7, and 10^8 CFU/mL. Following each injection of bacteria, five cycles of the following sequence are applied to the surface electrodes: 100 kHz 5 V_{pp} 10 s then 10 kHz 5 V_{pp} 10 s. Sensorgrams represent a one-minute rolling average and have been offset to zero (×) and baseline drift corrected (◯) before each injection. Each trace is a mean of 16-20 replicate regions, depending on immobilized species.

Bactenecin and penetratin regions were observed to monotonically increase in signal with increasing bacterial concentration. In contrast, magainin was found to interact very little to the presence of this strain of MRSA, in agreement with the findings of Pardoux *et al.*[26] Interestingly, the bactenecin derivative and cecropin A-melittin hybrid regions appear to yield similar signals upon injection of 10^6 and 10^7 CFU/mL, but increase significantly after injection of 10^8 CFU/mL.

Aside from the SPR response to injection of bacteria, significant modification of the plasmon curve was observed from the beginning of the experiment for the patterned electrodes relative to an unpatterned surface. The center of electrodes exhibited a plasmon curve with a useable linear region between 51° and 53°, while the electrode borders did not yield a plasmon effect within the range of angle swept by the SPR device (Figure 8). This marks a significant change to the plasmon curve relative to the unpatterned gold surface, which instead presents a reflectance minimum around 58° under the same experimental conditions (Supplementary Figure S3).

Surface plasmon propagation length is about 25 µm for 800 nm light. This places a limit on the spacing of electrodes, but only in the direction parallel to plasmon propagation.[23] This necessitates orienting the electrodes parallel to the direction of incident light.[43]

This observation is consistent with the increased thickness of electrode borders observed in SEM and profilometry. For the purposes of SPRi sensing, this did not present an issue since the borders are expected to interact with bacteria only during the pDEP interval. During the ACEO interval, bacteria are instead brought to the electrode centers, where plasmon resonance allows monitoring of surface phenomena at the chosen working angle.

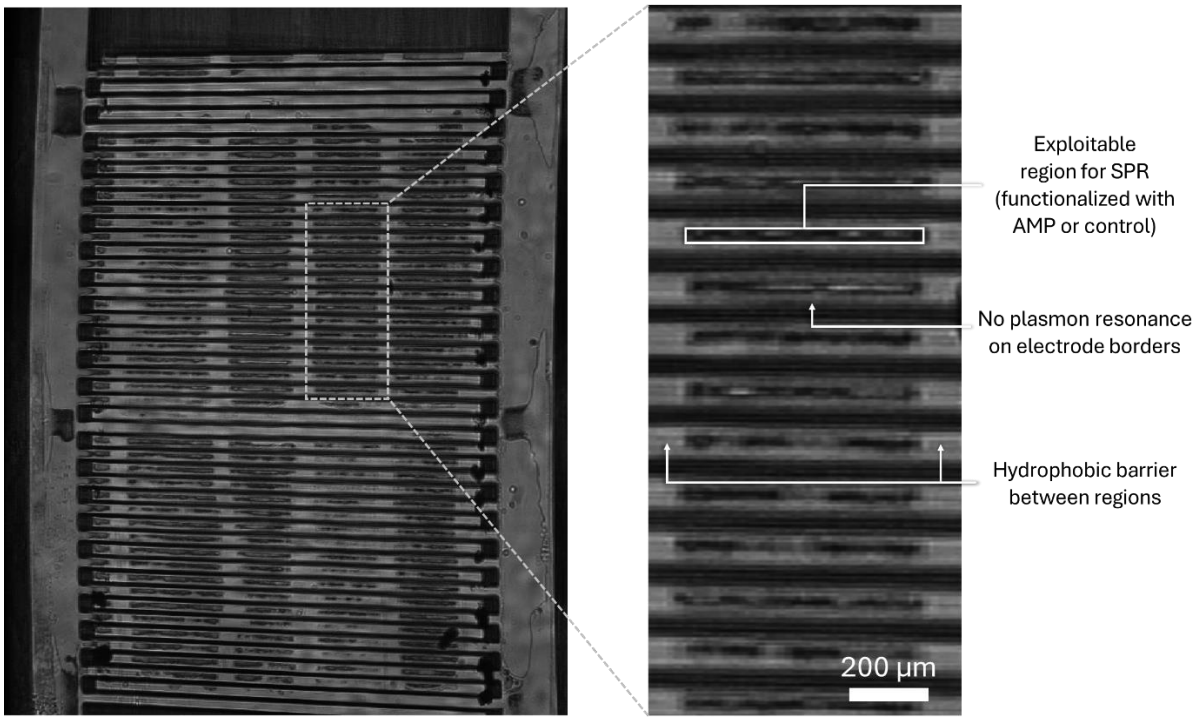

Figure 8 Left: The fabricated IDE array as observed by SPRi. Hydrophobic areas form a grid which delineate regions functionalized with different peptides. Right: Detail of one region, showing the plasmon resonance effect only in the center of each electrode.

Discussion

While laser ablation has been exploited for patterning of electrodes previously[21,22], the applicability of this method to the wider scientific community has to date been limited due to the hurdle of developing a custom optical setup. The advent of commercial LDW solutions democratizes access to this form of rapid prototyping, at least in terms of the skills required if not from a financial perspective. The presented method presupposes access to a PCB prototyper, which represents a significant up-front capital investment. Yet, in comparison to the cleanroom infrastructure, lithography equipment and chemical handling training necessary for traditional IDE fabrication methods, the purchase and maintenance of a PCB prototyper may still present cost savings in addition to the significant reduction in demands on a researcher's time.

While this work demonstrated the compatibility of laser patterning of IDE arrays with plasmonic biosensing, the results are presented as an alternative to traditional fabrication methods for these structures more generally. Due to a reliance on coupling of photons to surface plasmon polaritons, the SPR sensing method demonstrated in this work places especially stringent requirements on electrode smoothness and geometry, which may not apply for other applications of IDE arrays such as capacitive and impedimetric sensing. If the artifacts observed with only a contouring pass are not deemed problematic for a given application, an IDE array can be patterned in a gold surface in as little as 12 seconds with our method, which is difficult to improve upon even with the most rapid of alternative strategies. Electrodes of width 15 µm and larger can be easily achieved with this method, while retaining compatibility with popular gold-thiol conjugation chemistry.[19]

In this work, no attempt was made to modify the device control software, yet there are surely improvements to be made on our results if software-level limitations can be relaxed, for example by removing minimum allowable hatching overlaps.

These patterning results should be compared with IDEs produced by other rapid fabrication methods. One proposed alternative to lithography is inkjet printing of nanoparticles, as demonstrated by Tran *et al.*[16] While this method presents advantages such as being non-lithographic, maskless, and vacuum-free — the resulting electrode geometry was of much poorer quality than with our method, yielding much larger boundary ridges 40 µm in width and 42 nm thicker than the electrode center. Inkjet printing also necessitated a post-deposition curing step which a had a strong determinant effect on the conductivity, potentially introducing unwanted variability. Furthermore, the printer struggled to reproduce edges that were not aligned with the printhead direction, for example with curved boundaries. In comparison, the ability of the PCB prototyper beam to follow contours of the design geometry has an advantage since it does not introduce pixelation into the resulting pattern in the substrate, which may more faithfully reproduce curved or diagonal features.

Gaál *et al.* demonstrated IDE fabrication using fused deposition modelling (FDM) of graphene-doped thermoplastic.[17] While this method was rapid and produced IDEs in only six minutes, the electrodes are quite large in all dimensions with a thickness, width, and separation all on the order of 1 mm.

A further advantage of the method presented in this work is its feasibility not only for rapid prototyping, but also a moderate level of scalability to small volume production. Once a desired design has been identified, a single user can produce hundreds of patterned substrates in an afternoon with minimal changes to their workflow.

For example, with little regard for conserving material, we were able to create three different IDE array patterns, each with many different electrode spacings, into a single gold-coated microscope slide in as little as 10 minutes. By far the longest part of the fabrication workflow involved specifying the patterns in a CAD program, which can also be done in minutes.

SPRi prisms of the type used in this work are relatively expensive with a cost on the order of €100 per unit. For this reason, it is common practise to instead functionalize a cheaper gold-coated slide, which is then interfaced using an index matching gel with an un-metallized prism that is permanently mounted in an SPR device.[23] As shown in this work, the laser ablation method is compatible with both types of consumable.

During electro-trapping experiments, the observed progressive movement of bacteria towards the center of electrodes as applied frequency was reduced from 100 kHz to 10 kHz conforms with the frequency dependence of electro-osmotic velocity, which is maximal around 1 kHz and decreases almost to zero between 1 kHz and 100 kHz.[32]

The choice of 1.54 mmol NaCl as the carrier fluid was four-fold: it permitted a minimum mobile charge carrier density to enable ACEO[32], to yield pDEP within the desired frequency range, to minimize hypo-osmotic shock to the bacteria, and finally to minimize the oxidation of the gold film as a result of the applied alternating current.[14]

SPRi has previously been demonstrated for the specific detection of bacteria using arrays of immobilized antimicrobial peptides.[26] However, the time-to-results with this method was long, taking several hours to reveal interactions between AMPs and challenge bacteria.

We improved on this method by removing the diffusion limitations to SPR assay sensitivity.[9] This work directly showed detection of *S. aureus*, a realistic target analyte by virtue of its antibiotic resistance and status as a clinically relevant member of the ESKAPE group of pathogens.[44] A set of AMPs with known affinity to the challenge bacteria were chosen: bactenecin[38] and a bactenecin derivative[39], cecropin A-melittin[40], penetratin[41], and magainin[42]; and were immobilized using a method previously demonstrated elsewhere.[26]

The results of this work should be compared with previously demonstrated incorporation of electrokinetic mass transport into plasmonic sensors. A pair of articles have described a form of SPRi on an IDE arrays but stopped short of (bio)chemical functionalization of the electrodes for specific sensing.[9,10] Terao *et al.* recently demonstrated an electrokinetically active SPR sensor for the specific monitoring of molecular interactions, but dedicated the entire sensor surface to one probe and did not extend the technique to multiplexed SPRi.[14] The ability to monitor interactions between immobilized AMPs and bacteria with the patterned IDE array demonstrates the compatibility of this method of fabrication with SPRi sensing.

Conclusion

In this work we demonstrated the feasibility of leveraging commercial laser ablation equipment for rapid fabrication of micro-scale electrodes, yielding electrode widths from 111 µm down to 15 µm and electrode separation as small as 35 µm with total fabrication times as short as 12 seconds for a substrate area of 1 cm^2, with a potential for scaling to a very large surface area limited only by the 229×305 mm working area of the prototyper. It is a single-step, mask-free, and vacuum-free technique that requires no curing step or cleanroom infrastructure. Since no photolithography is performed, there is no danger of residual photoresist remaining on the surface which could

otherwise adversely affect the surface characteristics and interfere with (bio)chemical functionalisation.[19]

The method was then exploited for patterning of IDE arrays directly into gold-coated slides and off-the-shelf SPRi prisms. The patterned substrates were shown to be capable of electrokinetic mass transport of bacteria by dielectrophoresis and manipulation of the cells on the sensor surface by alternating current electro-osmosis.

The IDE arrays were then biofunctionalized with an array of various antimicrobial peptides and used to demonstrate for the first time the multiplexed biosensing of *S. aureus* by electrokinetic surface plasmon resonance imaging.

The fusion of rapid prototyping, electrokinetic manipulation, and plasmonic sensing represents an intriguing integration of mature and nascent technologies and opens up promising avenues for a new generation of electrokinetically active SPR sensors.

Author contributions

Author contributions The manuscript was written through contributions of all authors. All authors reviewed the manuscript and provided feedback. All authors have given approval to the final version of the manuscript.

Conceptualization— Larry O'Connell, Brice Poirier

Experimental work— Larry O'Connell, Brice Poirier, Oleksii Bratash, Charlène Plénière

Funding Acquisition— Pierre R. Marcoux, Yoann Roupioz

Investigation— Larry O'Connell, Brice Poirier

Resources— Pierre R. Marcoux, Yoann Roupioz

Software— Larry O'Connell

Supervision— Pierre R. Marcoux, Yoann Roupioz, Loïc Leroy

Validation— Pierre R. Marcoux, Yoann Roupioz

Original Draft Preparation— Larry O'Connell

Writing— Larry O'Connell

Review & Editing—Pierre R. Marcoux, Yoann Roupioz, Brice Poirier

Funding

This work has been partially supported by Labex ARCANE and CBH-EUR-GS (Grant ANR-17-EURE-0003).

Acknowledgments

The authors would like to thank:

Emmanuel Picard and Simon Glicenstein for assistance with microscopic observation of electro-trapping.

Hubert Teyssedre at Y.SPOT for assistance with laser ablation equipment.

Pierre-Henri Jouneau at CEA-Leti for assistance with electron microscopy.

All image credits are to the author unless otherwise stated. The authors would like to acknowledge the contribution of the Blender project (www.blender.org), without which the illustrations in this article would not have been possible.

Supplemental Information

Supplementary Table 1 Summary of immobilized antimicrobial peptides

Peptide	Storage buffer	Sequence	Tether	Ref.
Bactenecin	PBS + 5% glycerol	MPA-βA-βA-βA-RLARIVVIRVAR-NH_2	3-MPA	38
Bactenecin derivative	PBS + 5% glycerol	MPA-βA-βA-βA-RRWRIVVIRVRR-NH_2	3-MPA	39
Cecropin A-melittin	PBS + 5% glycerol	MPA-βA-βA-βA-KWKLFKKIGAVLKVL-NH_2	3-MPA	40
Penetratin	PBS + 5% glycerol	MPA-βA-βA-βA-RQIKIWFQNRRMKWKK-NH_2	3-MPA	41
Magainin	DMSO	GIGKFLHSAGKFGKAFVGEIMKS-AEEA-C-NH_2	L-cysteine amide	42

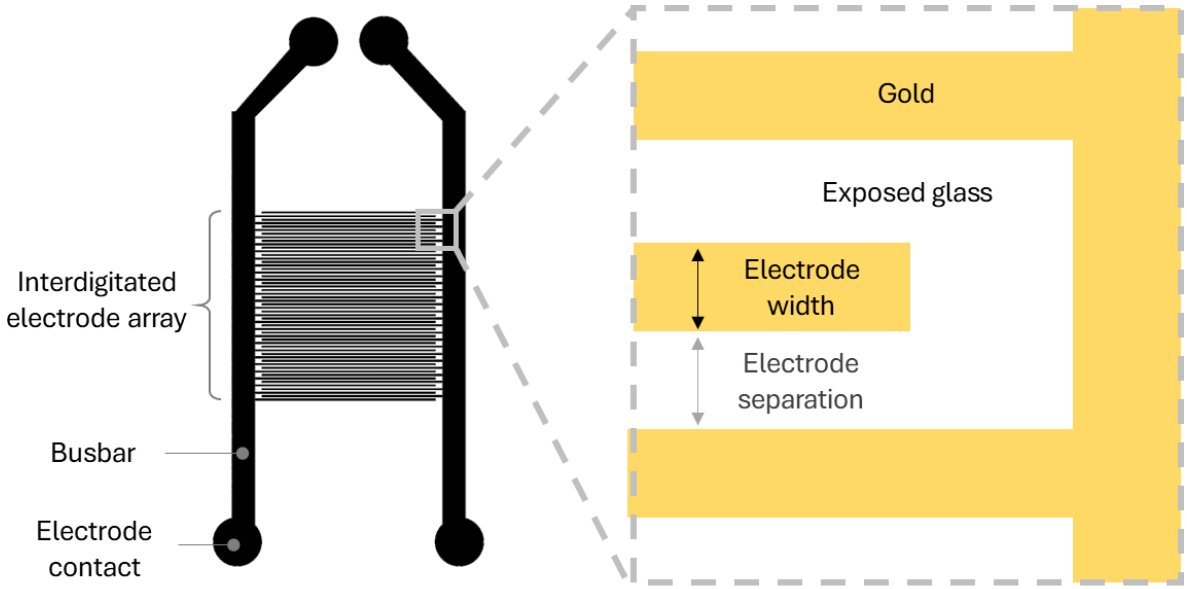

Supplemental Figure S1 Schematic of the pattern transferred to the substrate surface by laser patterning, featuring an array of 54 intermeshed electrodes of variable width and separation.

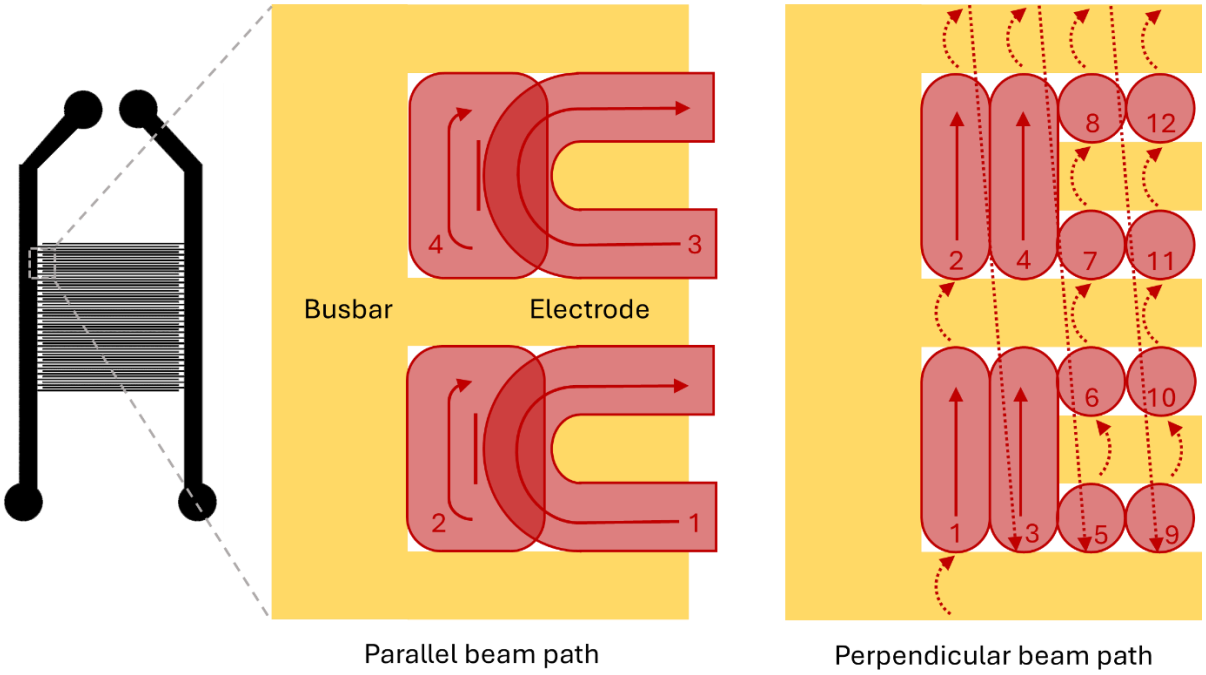

Supplementary Figure S2 Comparison of the parallel and perpendicular beam paths used in this work, so-named for the beam path orientation with respect to the long axis of electrode fingers. Numbers indicate the hypothetical order that each region would be exposed to the beam and are for illustrative purposes only. A parallel beam path was initially used but produced poor reproduction of the desired pattern. Surprisingly, a perpendicular beam path produced superior results.

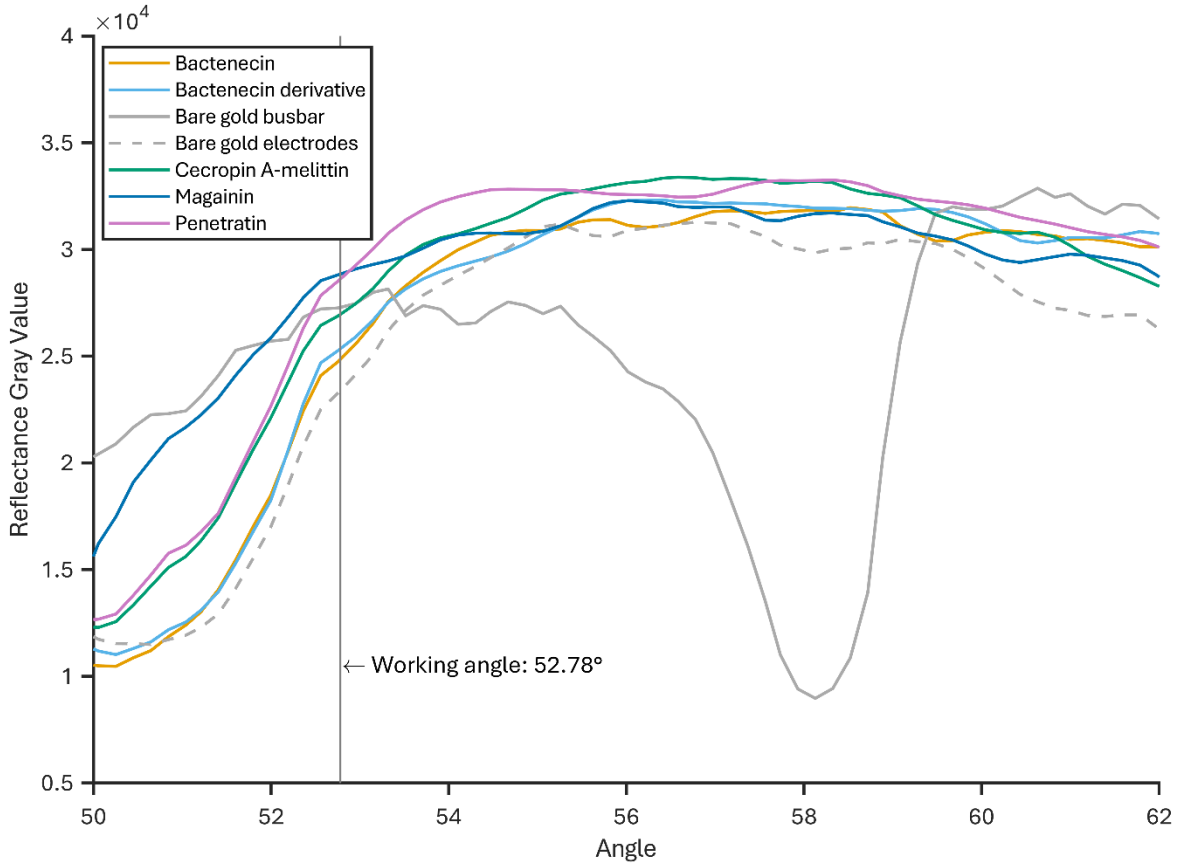

Supplementary Figure S3 Plasmon curves for all species. Each curve (except the gold busbar) is a mean of 16-20 replicate regions, depending on species. The reflectance minimum was strongly shifted relative to the un-patterned bare gold busbar surface (solid grey line).

Supplemental video S4 Patterning of prism surface in the PCB prototyper.

Supplemental video S5 Electro-trapping and displacement of bacteria on electrode surfaces

References

1. Ramanathan, S., Gopinath, S. C. B., Ismail, Z. H., Md Arshad, M. K. & Poopalan, P. Aptasensing nucleocapsid protein on nanodiamond assembled gold interdigitated electrodes for impedimetric SARS-CoV-2 infectious disease assessment. *Biosens. Bioelectron.* **197**, 113735 (2022) DOI: https://doi.org/https://doi.org/10.1016/j.bios.2021.113735.

2. Wang, L. *et al.* A sensitive DNA capacitive biosensor using interdigitated electrodes. *Biosens. Bioelectron.* **87**, 646–653 (2017) DOI: https://doi.org/10.1016/j.bios.2016.09.006.

3. Fiedler, S., Shirley, S. G., Schnelle, T. & Fuhr, G. Dielectrophoretic Sorting of Particles and Cells in a Microsystem. *Anal. Chem.* **70**, 1909–1915 (1998).

4. Alexander, F., Price, D. T. & Bhansali, S. Optimization of interdigitated electrode (IDE) arrays for impedance based evaluation of Hs 578T cancer cells. in *Journal of Physics: Conference Series* vol. 224 (2010). DOI: https://doi.org/10.1088/1742-6596/224/1/012134.

5. Dos Santos-Neto, I. S. *et al.* Interdigitated electrode for electrical characterization of commercial pseudo-binary biodiesel–diesel blends. *Sensors* **21**, (2021) DOI: https://doi.org/10.3390/s21217288.

6. Mazlan, N. S. *et al.* Interdigitated electrodes as impedance and capacitance biosensors: A review. *AIP Conf. Proc.* **1885**, (2017) DOI: https://doi.org/10.1063/1.5002470.

7. Tsouti, V., Boutopoulos, C., Zergioti, I. & Chatzandroulis, S. Capacitive microsystems for biological sensing. *Biosens. Bioelectron.* **27**, 1–11 (2011) DOI: https://doi.org/10.1016/j.bios.2011.05.047.

8. Khan, R. R. & Kang, S. W. Highly sensitive multi-channel IDC sensor array for low concentration taste detection. *Sensors (Switzerland)* **15**, 13201–13221 (2015) DOI: https://doi.org/10.3390/s150613201.

9. Avenas, Q. *et al.* Performance improvement of plasmonic sensors using a combination of AC electrokinetic effects for (bio)target capture. *Electrophoresis* **40**, 1426–1435 (2019) DOI: https://doi.org/10.1002/elps.201800436.

10. Costella, M. *et al.* Dielectrophoretic cell trapping for improved surface plasmon resonance imaging sensing. *Electrophoresis* **40**, 1417–1425 (2019) DOI: https://doi.org/10.1002/elps.201800439.

11. Batra, N., Ansari, M. A., Singh, S. & Urooj, S. Fabrication of Interdigitated Electrodes based biosensor and Prediction of Covid-19 cases using Linear Regression. *Int. J. Disaster Recover. Bus. Contin.* **11**, 2514–2527 (2020).

12. Madou, M. J. Volume 2 Part I: Lithography. in *Fundamentals of Microfabrication and Nanotechnology* (CRC Press, 2011).

13. Hart, C. *et al.* Rapid nanofabrication of nanostructured interdigitated electrodes (NIDES) for long-term in vitro analysis of human induced pluripotent stem cell differentiated cardiomyocytes. *Biosensors* **8**, 1–10 (2018) DOI: https://doi.org/10.3390/bios8040088.

14. Terao, K. & Kondo, S. AC-Electroosmosis-Assisted Surface Plasmon Resonance Sensing for Enhancing Protein Signals with a Simple Kretschmann Configuration. *Sensors* **22**, (2022) DOI: https://doi.org/10.3390/s22030854.

15. Colniță, A., Marconi, D. & Turcu, I. Fabrication of Interdigitated Electrodes using Molecular

Beam Epitaxy and Optical Lithography. *Anal. Lett.* **49**, 378–386 (2016) DOI: https://doi.org/10.1080/00032719.2015.1033719.

16. Tran, V. T., Wei, Y., Liau, W. J., Yang, H. & Du, H. Preparing of interdigitated microelectrode arrays for AC electrokinetic devices using inkjet printing of silver nanoparticles ink. *Micromachines* **8**, (2017) DOI: https://doi.org/10.3390/mi8040106.

17. Gaál, G. *et al.* 3D printed e-tongue. *Front. Chem.* **6**, 1–8 (2018) DOI: https://doi.org/10.3389/fchem.2018.00151.

18. Contreras-Saenz, M., Hassard, C., Vargas-Chacon, R., Gordillo, J. L. & Camacho-Leon, S. Maskless fabrication of a microfluidic device with interdigitated electrodes on PCB using laser ablation. in *Proc. SPIE 9705, Microfluidics, BioMEMS, and Medical Microsystems XIV, 97050N* vol. 9705 18–24 (2016). DOI: https://doi.org/10.1117/12.2222961.

19. O'Connell, L., Marcoux, P. R. & Roupioz, Y. Strategies for Surface Immobilization of Whole Bacteriophages: A Review. *ACS Biomater. Sci. Eng.* **7**, 1987–2014 (2021) DOI: https://doi.org/10.1021/acsbiomaterials.1c00013.

20. Love, J. C., Estroff, L. A., Kriebel, J. K., Nuzzo, R. G. & Whitesides, G. M. *Self-Assembled Monolayers of Thiolates on Metals as a Form of Nanotechnology*. *Chem. Rev.* vol. 105 (2005). DOI: https://doi.org/10.1021/cr0300789.

21. Tender, L. M., Worley, R. L., Fan, H. & Lopez, G. P. Electrochemical Patterning of Self-Assembled Monolayers onto Microscopic Arrays of Gold Electrodes Fabricated by Laser Ablation. *Langmuir* **12**, 5515–5518 (1996) DOI: https://doi.org/10.1021/la960627o.

22. Manzoli, A. *et al.* Femtosecond laser ablation of gold interdigitated electrodes for electronic tongues. *Opt. Laser Technol.* **69**, 148–153 (2015) DOI: https://doi.org/10.1016/j.optlastec.2014.12.026.

23. Schasfoort, R. B. M. *Handbook of Surface Plasmon Resonance*. (Royal Society of Chemistry, 2017). doi:10.1039/9781788010283 DOI: https://doi.org/10.1039/9781788010283.

24. Homola, J. Surface plasmon resonance sensors for detection of chemical and biological species. *Chem. Rev.* **108**, 462–493 (2008) DOI: https://doi.org/10.1021/cr068107d.

25. Hurot, C. *et al.* Highly sensitive olfactory biosensors for the detection of volatile organic compounds by surface plasmon resonance imaging. *Biosens. Bioelectron.* **123**, 230–236 (2019) DOI: https://doi.org/10.1016/j.bios.2018.08.072.

26. Pardoux, É., Roux, A., Mathey, R., Boturyn, D. & Roupioz, Y. Antimicrobial peptide arrays for wide spectrum sensing of pathogenic bacteria. *Talanta* **203**, 322–327 (2019) DOI: https://doi.org/10.1016/j.talanta.2019.05.062.

27. Barik, A. *et al.* Dielectrophoresis-enhanced plasmonic sensing with gold nanohole arrays. *Nano Lett.* **14**, 2006–2012 (2014) DOI: https://doi.org/10.1021/nl500149h.

28. Song, Y. *et al.* AC Electroosmosis-Enhanced Nanoplasmofluidic Detection of Ultralow-Concentration Cytokine. *Nano Lett.* **17**, 2374–2380 (2017) DOI: https://doi.org/10.1021/acs.nanolett.6b05313.

29. Tai, Y. H., Chang, D. M., Pan, M. Y., Huang, D. W. & Wei, P. K. Sensitive detection of small particles in fluids using optical fiber tip with dielectrophoresis. *Sensors* **16**, 1–9 (2016) DOI: https://doi.org/10.3390/s16030303.

30. Cottet, J. *et al.* MyDEP: A New Computational Tool for Dielectric Modeling of Particles and Cells. *Biophys. J.* **116**, 12–18 (2019) DOI: https://doi.org/10.1016/j.bpj.2018.11.021.

31. Gagnon, Z. R. Cellular dielectrophoresis: Applications to the characterization, manipulation, separation and patterning of cells. *Electrophoresis* **32**, 2466–2487 (2011) DOI: https://doi.org/10.1002/elps.201100060.

32. Green, N. G., Ramos, A., González, A., Morgan, H. & Castellanos, A. Fluid flow induced by nonuniform ac electric fields in electrolytes on microelectrodes. I. Experimental measurements. *Phys. Rev. E - Stat. Physics, Plasmas, Fluids, Relat. Interdiscip. Top.* **61**, 4011–4018 (2000) DOI: https://doi.org/10.1103/PhysRevE.61.4011.

33. Ramos, A., Morgan, H., Green, N. G. & Castellanos, A. AC electric-field-induced fluid flow in microelectrodes. *J. Colloid Interface Sci.* **217**, 420–422 (1999) DOI: https://doi.org/10.1006/jcis.1999.6346.

34. Kim, J. & Na, S. Metal thin film ablation with femtosecond pulsed laser. *Opt. Laser Technol.* **39**, 1443–1448 (2007) DOI: https://doi.org/10.1016/j.optlastec.2006.10.001.

35. Radke, S. M. & Alocilja, E. C. Design and fabrication of a microimpedance biosensor for bacterial detection. *IEEE Sens. J.* **4**, 434–440 (2004) DOI: https://doi.org/10.1109/JSEN.2004.830300.

36. Laczka, O., Baldrich, V., Muñoz, F. X. & Campo, J. del. Detection of Escherichia coli and Salmonella typhimurium Using Interdigitated Microelectrode Capacitive Immunosensors: The Importance of Transducer Geometry. *Anal. Chem.* **80**, 7239–7247 (2008).

37. Schaffer, C. B., Brodeur, A., García, J. F. & Mazur, E. Micromachining bulk glass by use of femtosecond laser pulses with nanojoule energy. *Opt. Lett.* **26**, 93–95 (2001).

38. Romeo, D., Skerlavaj, B., Bolognesi, M. & Gennaro, R. Structure and bactericidal activity of an antibiotic dodecapeptide purified from bovine neutrophils. *J. Biol. Chem.* **263**, 9573–9575 (1988) DOI: https://doi.org/10.1016/s0021-9258(19)81553-3.

39. Hilpert, K., Volkmer-Engert, R., Walter, T. & Hancock, R. E. W. High-throughput generation of small antibacterial peptides with improved activity. *Nat. Biotechnol.* **23**, 1008–1012 (2005) DOI: https://doi.org/10.1038/nbt1113.

40. Andreu, D. *et al.* Shortened cecropin A-melittin hybrids Significant size reduction retains potent antibiotic activity. *FEBS Lett.* **296**, 190–194 (1992) DOI: https://doi.org/10.1016/0014-5793(92)80377-S.

41. Derossi, D., Joliot, A. H., Chassaing, G. & Prochiantz, A. The third helix of the Antennapedia homeodomain translocates through biological membranes. *J. Biol. Chem.* **269**, 10444–10450 (1994) DOI: https://doi.org/10.1016/s0021-9258(17)34080-2.

42. Zasloff, M. Magainins, a class of antimicrobial peptides from Xenopus skin: Isolation, characterization of two active forms, and partial cDNA sequence of a precursor. *Proc. Natl. Acad. Sci. U. S. A.* **84**, 5449–5453 (1987) DOI: https://doi.org/10.1073/pnas.84.15.5449.

43. Galvan, D. D., Parekh, V., Liu, E., Liu, E. L. & Yu, Q. Sensitive Bacterial Detection via Dielectrophoretic-Enhanced Mass Transport Using Surface-Plasmon-Resonance Biosensors. *Anal. Chem.* **90**, 14635–14642 (2018) DOI: https://doi.org/10.1021/acs.analchem.8b05137.

44. Rice, L. B. Federal funding for the study of antimicrobial resistance in nosocomial pathogens: No ESKAPE. *J. Infect. Dis.* **197**, 1079–1081 (2008) DOI: https://doi.org/10.1086/533452.

Vitae

Larry O'Connell

Larry O'Connell received his BA (Hons.) in Physics from Trinity College Dublin (Ireland) in 2013 and a master's degree with distinction in Nanoscale Engineering from l'Institut National des Sciences Appliquées de Lyon (France) in 2017. He is pursuing a PhD from Université Grenoble-Alpes with the specialty Biotechnology, instrumentation, signal and imaging for biology, medicine, and the environment. His doctoral research was carried out at Systèmes Moléculaires et nanoMatériaux pour l'Énergie et la Santé (IRIG, Grenoble, France) and Laboratory of Imaging systems for Health (CEA, Grenoble, France). His many research interests include microfluidics and biosensing.

Brice Poirier

Brice Poirier graduated from the HTGAA program in bioengineering and synthetic biology hosted by the MIT Media Lab in 2017. He led a fablab in Paris-Saclay, focused on user-centric services, tech for good and led workshops on Man-Machine Interfaces. In 2019, he became the fabmanager of l'Atelier, the CEA Open Innovation Center in Grenoble where he supported scientists in the design and fabrication of experimental setups, more efficient fabrication protocols and focused on COVID-oriented projects. He is now an Open Innovation Project Manager in Montpellier. Among others, his research interests are phytoremediation and ethics in genetic engineering.

Oleksii Bratash

Oleksii Bratash received his BS degree in Applied Physics in 2016 and MS degree with honors in Applied Physics and Nanomaterials in 2019 from Taras Shevchenko National University of Kyiv (Ukraine). He obtained the second MS degree in Nanoscale Engineering from Ecole Centrale de Lyon (France) in 2019. He is pursuing a PhD in Biosensing, Interferometry, and optical instrumentation from Université Grenoble-Alpes, with experimental work performed at the Interdisciplinary Research Institute of Grenoble (IRIG) and at CEA Grenoble, France. The main research interests: biosensing, interferometry, optical fibers, surface chemistry.

Charlène Plénière

Charlène Plénière graduated from l'Université de Bretagne Sud with a bachelor's degree in Biotechnology in 2017. She then obtained an engineering degree in Microbiology and Quality at l'Ecole Supérieure d'Ingénieurs en Agroalimentaire de Bretagne as well as a master's degree in Fundamental and Applied Microbiology at l'Université de Bretagne Occidentale, in 2020. She is now working at the Systèmes Moléculaires et nanoMatériaux pour l'Énergie et la Santé (IRIG, Grenoble, France) on characterization and validation of a biosensor dedicated to the study of pathogenic bacteria from human blood. Her research interests are microbial behavior and biosensors.

Loïc Leroy

Loïc Leroy, born in 1975, is an associate professor in UGA (Université Grenoble Alpes) since 2006. His research mainly focuses on the development of biophysical instrumentation (high resolution plasmonics and combined optical methods) for label-free cell and bacteria studies. He also works on localized electrochemistry, optical functionalization, and optical fibers for biochip design.

Pierre

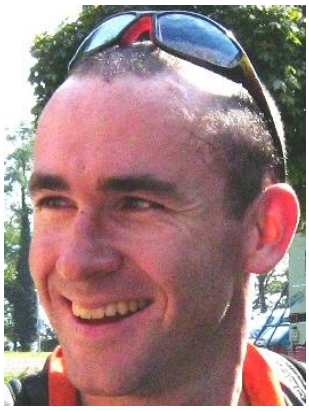

Pierre R. Marcoux is chemist in CEA – LETI (Grenoble, France). His background in colloid science and chemistry of nanomaterials leads him to develop innovative ways of characterizing phages, from a physicochemical point of view (*e.g.,* zeta potential, buoyant mass, refractive index, light scattering, hydrodynamic radius). His current research also deals with rapid phenotypic methods in diagnostic microbiology, especially based on optical methods (*e.g.*, multispectral imaging, elastic light scattering, vibrational spectroscopies).

Yoann Roupioz

Dr. Yoann Roupioz graduated from the Chemistry Department of the University of Montreal, Canada, in 1997. He returned to France and received his PhD degree in 2001 at the University of Grenoble-Alpes, in the Nucleic Acids chemistry. He then went to the University of British Columbia, Canada, to work on catalytic Nucleic Acids (2001-2002), and at the French Nuclear Energy Office in Paris (2002-2004) where he focused on living cell micro-arrays. Since 2005, Yoann is Researcher for the French National Center for Scientific Research (CNRS) and is developing cell-based biosensors at CEA, Grenoble.

Declaration of interests

☒The authors declare that they have no known competing financial interests or personal relationships that could have appeared to influence the work reported in this paper.

☐The authors declare the following financial interests/personal relationships which may be considered as potential competing interests:

Click here to access/download
Supplementary Material
Supplemental video S4.mov

Click here to access/download
Supplementary Material
Supplemental video S5.avi